AD-787 655

INFLUENCE OF YIELD STRENGTH ON OVERLOAD AFFECTED
FATIGUE CRACK GROWTH BEHAVIOR IN 4340 STEEL

AIR FORCE FLIGHT DYNAMICS LABORATORY

JULY 1974

NOTICE

When Government drawings, specifications, or other data are used for any purpose other than in connection with a definitely related Government procurement operation, the United States Government thereby incurs no responsibility nor any obligation whatsoever; and the fact that the government may have formulated, furnished, or in any way supplied the said drawings, specifications, or other data, is not to be regarded by implication or otherwise as in any manner licensing the holder or any other person or corporation, or conveying any rights or permission to manufacture, use, or sell any patented invention that may in any way be related thereto.

Copies of this report should not be returned unless return is required by security considerations, contractual obligations, or notice on a specific document.

AD 787655

DOCUMENT CONTROL DATA - R & D

Security classification of title, body of abstract and indexing annotation must be entered when the overall report is classified)

1. ORIGINATING ACTIVITY (Corporate author)	2a. REPORT SECURITY CLASSIFICATION
Air Force Flight Dynamics Laboratory Wright-Patterson Air Force Base, Ohio	UNCLASSIFIED 2b. GROUP

3. REPORT TITLE

INFLUENCE OF YIELD STRENGTH ON OVERLOAD AFFECTED FATIGUE CRACK GROWTH BEHAVIOR IN 4340 STEEL

4. DESCRIPTIVE NOTES (Type of report and inclusive dates)

Final Report February 1973 through February 1974

5. AUTHOR(S) (First name, middle initial, last name)

J. P. Gallagher
T. F. Hughes

6. REPORT DATE	7a. TOTAL NO. OF PAGES	7b. NO. OF REFS
July 1974		15

8a. CONTRACT OR GRANT NO.	9a. ORIGINATOR'S REPORT NUMBER(S)
b. PROJECT NO. 1467	AFFDL-TR-74-27
Work Unit 13470413	9b. OTHER REPORT NO(S) (Any other numbers that may be assigned this report)

10. DISTRIBUTION STATEMENT

Approved for public release; distribution unlimited

11. SUPPLEMENTARY NOTES	12. SPONSORING MILITARY ACTIVITY
	Air Force Flight Dynamics Laboratory (FBR) Wright-Patterson Air Force Base, Ohio 45433

13. ABSTRACT

Single tensile overloads were applied to 4340 steel specimens which were treated to give 120 and 220 ksi yield strength levels. The influence of yield strength level on the number of nonsteady state crack growth cycles subsequent to the application of a 100 percent overload was noted to be substantial. The number of nonsteady state cycles for the 120 ksi yield strength steel was approximately an order of magnitude greater than that of the higher strength steel. A retardation model was developed using a residual stress intensity factor concept similar to that proposed by Willenborg et al. The model was found to predict to within 10 percent the number of nonsteady state crack growth cycles required to move a crack from the pre-overload position to a subsequent position, one overload induced plane stress plastic zone radius ahead of the pre-overload position. The model indicates that the reason for substantial increases in nonsteady state crack growth cycles observed for the low strength steel is due to a corresponding increase in the overload affected zone size.

14 KEY WORDS	LINK A		LINK B		LINK C	
	ROLE	WT	ROLE	WT	ROLE	WT
Fatigue Crack Growth						
Fracture Mechanics						
Single Overloads						
Yield Strength						
Retardation Modeling						

12

INFLUENCE OF YIELD STRENGTH ON
OVERLOAD AFFECTED FATIGUE CRACK GROWTH BEHAVIOR
IN 4340 STEEL

J. P. Gallagher
and
T. F. Hughes

FOREWORD

This report is the result of an in-house effort under Project 1467, "Analysis Methods for Military Flight Vehicle Structures," Work Unit 13470413, "Experimental Studies in Fatigue Crack Propagation in USAF Aerospace Structures." The work was conducted in the Air Force Flight Dynamics Laboratory at Wright-Patterson Air Force Base, Ohio by Dr. J. P. Gallagher, and Mr. T. F. Hughes (FBR). The effort covered the time period of February 1973 through February 1974.

Mr. Robert Mayle was responsible for the collection of the 120 ksi yield strength steel crack growth measurements and Mr. James Weirer collected the crack growth data for the 220 ksi yield strength steel. Mr. F. Hussong is acknowledged for his contributions in developing the crack measurement system utilized in this investigation. Mr. I. D. Hearne and Mr. H. D. Stalnaker were principally responsible for developing the test system. All tests were conducted in the Experimental Branch Test Facility (Bldg.65) which is under the direction of Mr. R. Cavanaugh.

This report was submitted by the authors February 1974.

This Technical Report has been reviewed and is approved.

FRANCIS J. JANIK JR.
Chief, Solid Mechanics Branch
Structures Division

ABSTRACT

Single tensile overloads were applied to 4340 steel specimens which were heat treated to give 120 and 220 ksi yield strength levels. The influence of yield strength level on the number of nonsteady state crack growth cycles subsequent to the application of a 100 percent overload was noted to be substantial. The number of nonsteady state cycles for the 120 ksi yield strength steel was approximately an order of magnitude greater than that of the higher strength steel. A retardation model was developed using a residual stress intensity factor concept similar to that proposed by Willenborg et. al. The model was found to predict to within 10 percent the number of nonsteady state crack growth cycles required to move a crack from the pre-overload position to a subsequent position, one overload induced plane stress plastic zone radius ahead of the pre-overload position. The model indicates that the reason for substantial increases in nonsteady state crack growth cycles observed for the low strength steel is due to a corresponding increase in the overload affected zone size.

TABLE OF CONTENTS

Preceding page blank

LIST OF FIGURES

LIST OF TABLES

LIST OF SYMBOLS

a	Crack length
a_o, a_f	Initial and final crack length
a^*	Overload affected crack length
a^*_{avg}	Average of 8 or 9 a^* measured values
a_{OL}	Defines crack position immediately prior to the overload cycle
b	Constant (see Equation 16)
Δa	Crack movement from a_{OL}
a_s, a_{int}	Δa measured on specimen surface and specimen mid-plane (post-fracture), respectively
$\frac{da}{dN}$	Cyclic crack growth rate
$\left.\frac{da}{dN}\right\|_{ss}$	Measured steady state cyclic crack growth rate
C, p	Empirical constants associated with Paris power law crack growth equation (Equation 12)
δ_{int}	Discrete crack movements associated with overload
K	Remote stress intensity factor
K^{eff}	Effective stress intensity factor (Equation 1)
K^{OL}	K associated with overload
K_{max}, K_{min}	Maximum and minimum K
$K^{eff}_{max}, K^{eff}_{min}$	Maximum and minimum K^{eff}
$K^{OL}_{max}, K^{OL}_{min}$	Maximum and minimum K^{OL}
K_R	Residual stress intensity factor
K^W_R	Willenborg et al assumed K_R
K^+	K used to establish estimate of a^*

LIST OF SYMBOLS

a	Crack length
a_0, a_f	Initial and final crack length
a^*	Overload affected crack length
a^*_{avg}	Average of 8 or 9 a^* measured values
a_{OL}	Defines crack position immediately prior to the overload cycle
A	Constant (see Equation 16)
Δa	Crack movement from a_{OL}
$\Delta a_s, \Delta a_{int}$	Δa measured on specimen surface and specimen mid-plane (post-fracture), respectively
$\dfrac{\Delta a}{\Delta N}$	Cyclic crack growth rate
$\left.\dfrac{\Delta a}{\Delta N}\right|_{ss}$	Measured steady state cyclic crack growth rate
C, p	Empirical constants associated with Paris power law crack growth equation (Equation 12)
δ_{int}	Discrete crack movements associated with overload
K'	Remote stress intensity factor
K^{eff}	Effective stress intensity factor (Equation 1)
K^{OL}	K' associated with overload
K'_{max}, K'_{min}	Maximum and minimum K'
$K^{eff}_{max}, K^{eff}_{min}$	Maximum and minimum K^{eff}
$K^{OL}_{max}, K^{OL}_{min}$	Maximum and minimum K^{OL}
K_R	Residual stress intensity factor
K_R^W	Willenborg et al assumed K_R
K^+	K^{α} used to establish estimate of a^*

LIST OF SYMBOLS (CONT)

K^*	Initial no retardation stress intensity factor
K^{**}	Subsequent higher level no retardation stress intensity factor
$K_{max_{TH}}$	Threshold maximum stress intensity factor for no fatigue growth, $R^\infty = 0$
ΔK	Stress intensity factor range $(K_{max}^\omega - K_{min}^\infty)$
ΔK_{eff}	An effective stress intensity factor range

$$(= K_{max}^{eff} - K_{min}^{eff}, \ K_{min}^{eff} > 0; \ = K_{max}^{eff}, \ K_{min}^{eff} \le 0)$$

N	Number of cycles
N_{OL}, N^ω	Number of overload cycles and subsequent lower level cycles
N^*	N^ω required to propagate crack from a_{OL} to $a_{OL} + a^*$
N^{**}	N^ω required to propagate crack from a_{OL} to $a_{OL} + r_{y_{OL}}$
N_W	Willenborg et al predicted N^{**}
N_M	New model predicted N^{**}
R^ω	Stress ratio $(K_{min}^\omega / K_{max}^\omega)$
$r_{y_{OL}}$	Plane stress plastic zone radius
$r^*_{y_{OL}}$	Plane strain plastic zone radius
r_o	Plastic zone diameter
X	Fraction of shear lips on fracture surface cross section
z	Load interaction zone

LIST OF SYMBOLS (CONT)

K^*	Initial no retardation stress intensity factor
K^{**}	Subsequent higher level no retardation stress intensity factor
$K_{max_{TH}}$	Threshold maximum stress intensity factor for no fatigue growth, $R^\infty = 0$
ΔK	Stress intensity factor range $(K_{max}^\infty - K_{min}^\infty)$
ΔK_{eff}	An effective stress intensity factor range $(= K_{max}^{eff} - K_{min}^{eff}, \ K_{min}^{eff} > 0; \ = K_{max}^{eff}, \ K_{min}^{eff} \leq 0)$
N	Number of cycles
N_{OL}, N^∞	Number of overload cycles and subsequent lower level cycles
N^*	N^∞ required to propagate crack from a_{OL} to $a_{OL} + a^*$
N^{**}	N^∞ required to propagate crack from a_{OL} to $a_{OL} + r_{y_{OL}}$
N_W	Willenborg et al predicted N^{**}
N_M	New model predicted N^{**}
R^∞	Stress ratio $(K_{min}^\infty / K_{max}^\infty)$
$r_{y_{OL}}$	Plane stress plastic zone radius
$r^*_{y_{OL}}$	Plane strain plastic zone radius
r_o	Plastic zone diameter
X	Fraction of shear lips on fracture surface cross section
z	Load interaction zone

LIST OF SYMBOLS (CONT)

z_{OL} Overload z

$\vdots$ A retardation constant determined by overload shut-off
                  of subsequent growth

SECTION I

INTRODUCTION

Variable amplitude load spectra when applied to cracked structures result in observations of crack movement which are at variance with simple no-load-interaction crack growth prediction techniques. One recognized facet of the crack growth behavior generated under spectrum loading is that substantially slower crack growth rates are observed when small amplitude load cycles are preceded by a load level with a higher maximum.

Several crack growth retardation models have been developed to predict this high-low load interaction effect. Wheeler (Reference 1) provided a model which identified the concept of a load interaction zone. He derived this model assuming that the ratio of interaction zones is directly related to the observed decrease in crack growth rates. Willenborg et al (Reference 2) used the Wheeler formulation of load interaction zones to derive a model which was based on the difference between load interaction zone sizes. Both of the above mentioned models were reformulated by Gallagher (Reference 3) to help identify the physical implications as well as to provide identifiable modeling forms for others who are directing their attention to a residual stress intensity factor concept.

The use of a residual stress intensity factor concept suggests that the local or effective stress intensity factor which is sensed by the propagating crack be calculated from

$$K^{eff} = K^{\alpha} - K_R \tag{1}$$

where K^{α} is the stress intensity factor associated with remotely applied loads. The residual stress intensity factor (K_R) would in general be considered a function of many interacting variables, e.g.:

$$K_R = f \ (K_{max}^{OL}, \ K_{min}^{OL}, \ N_{OL}, \ K_{max}^{\infty}, \ R^{\infty}, \sigma_{ys}, N^{\infty}, \ \dots) \tag{2}$$

where $\quad K_{max}^{OL}$ = maximum K^{∞} generated by the overload

$\qquad K_{min}^{OL}$ = minimum K^{∞} generated by the overload

$\qquad N_{OL}$ = number of overloads applied

$\qquad K_{max}^{\infty}$ = maximum K^{∞} generated by the loads following the overload

$\qquad R^{\infty}$ = stress ratio of remotely applied loads

$\qquad N^{\infty}$ = number of cycles of K_{max}^{∞}

$\qquad \sigma_{ys}$ = yield strength level

SECTION II

TEST METHODS AND MATERIALS

1. MATERIALS AND SPECIMEN GEOMETRY

The nominal chemical composition of the one-half inch thick 4340 steel specimens which were employed in this investigation is given in Table I and the heat treatment schedules used to produce the 220 ksi and 120 ksi yield strength levels are given in Table II.

The geometry of the specimens is shown in Figure 1 and the corresponding stress intensity factor coefficient is given in Figure 2 from Reference 4.

2. TEST TECHNIQUES

A constant stress intensity factor condition was held throughout the tests such that an overload stress intensity factor K_{max}^{OL} of 40 ksi $\sqrt{in}$ was followed by repeated cyclic load applications corresponding to a remotely calculated stress intensity factor varying between 2 and 20 ksi $\sqrt{in}$. The condition: K_{max}^{OL} = 40 ksi $\sqrt{in}$, K_{max}^{α} = 20 ksi $\sqrt{in}$, K_{min}^{α} = 2 ksi $\sqrt{in}$ was applied repeatedly to specimens heat treated to the two yield strength levels while observations of crack length movement were made. Prior to a reapplication of an overload, it was determined that the cracking rates associated with the K_{max}^{α} = 20 ksi $\sqrt{in}$ condition were steady state and no longer appeared to be influenced by the previously applied overload.

A schedule of loads for any 0.025 inch increment on the crack path, as required by Figure 2 to achieve the desired constant stress intensity conditions, was developed prior to test start up and then utilized during the test. It was normally possible to define the surface crack position to within a 0.0005 inch tolerance since crack length measurements were made using a 20X Gaertner microscope mounted on a 1.0 inch Aerotech translation stage which was remotely controlled to move in 0.0001 inch increments.

TABLE I

NOMINAL CHEMICAL COMPOSITION OF 4340 STEEL

C	Mn	P	Si	Ni	Cr	Mo	Fe
0.40	0.72	0.012	0.28	1.70	0.80	0.24	Remainder

TABLE II

HEAT TREATMENT SCHEDULE FOR 4340 STEEL SPECIMENS

FOR 220 KSI YIELD STRENGTH

1. Austenitize 1600°F for 1 hour in salt bath

2. Oil Quench

3. Temper 1 hour at 600°F in air

4. Water cool

5. Repeat steps 3 and 4

6. Surface grind, remove 0.020 in. from both sides of the specimen

FOR 120 KSI YIELD STRENGTH

1. Repeat steps 1 thru 6 (220 ksi yield strength)

2. Anneal at 1550°F for 1 hour in air

3. Slow cool specimen in sand from 1550°F to ambient temperature
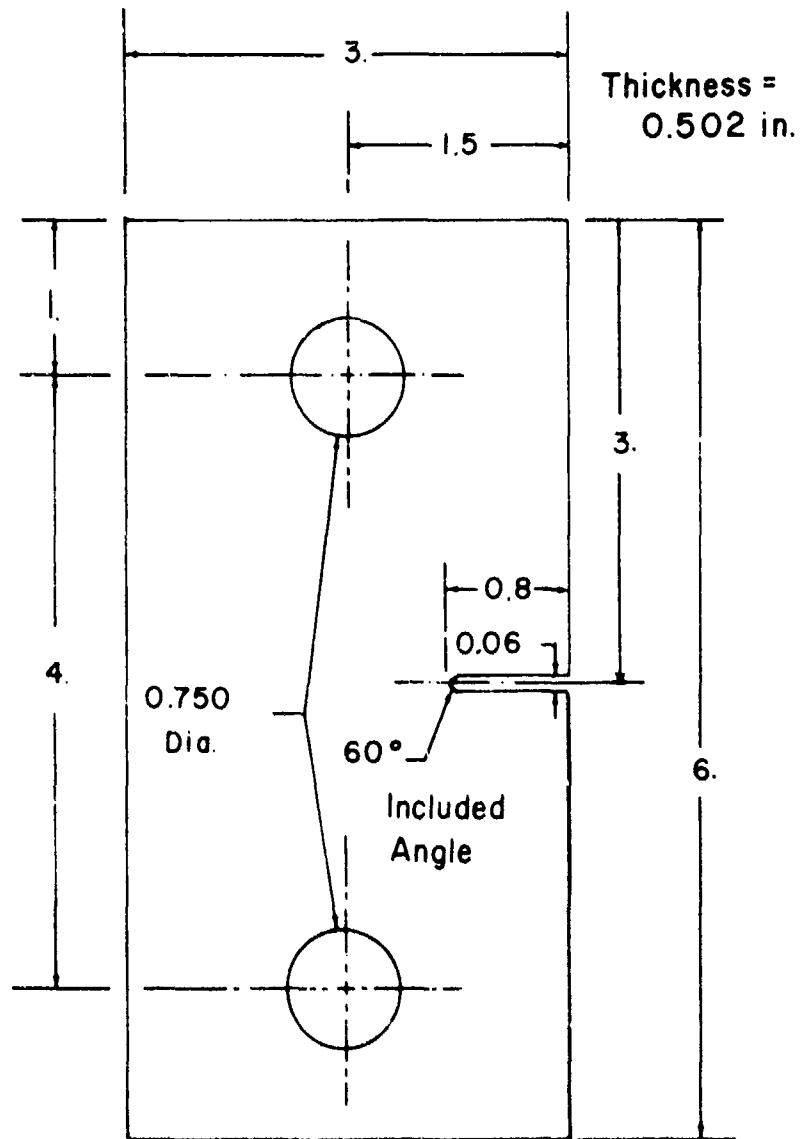
Figure 1. Geometry of Single Edge Notch (SEN) Specimen
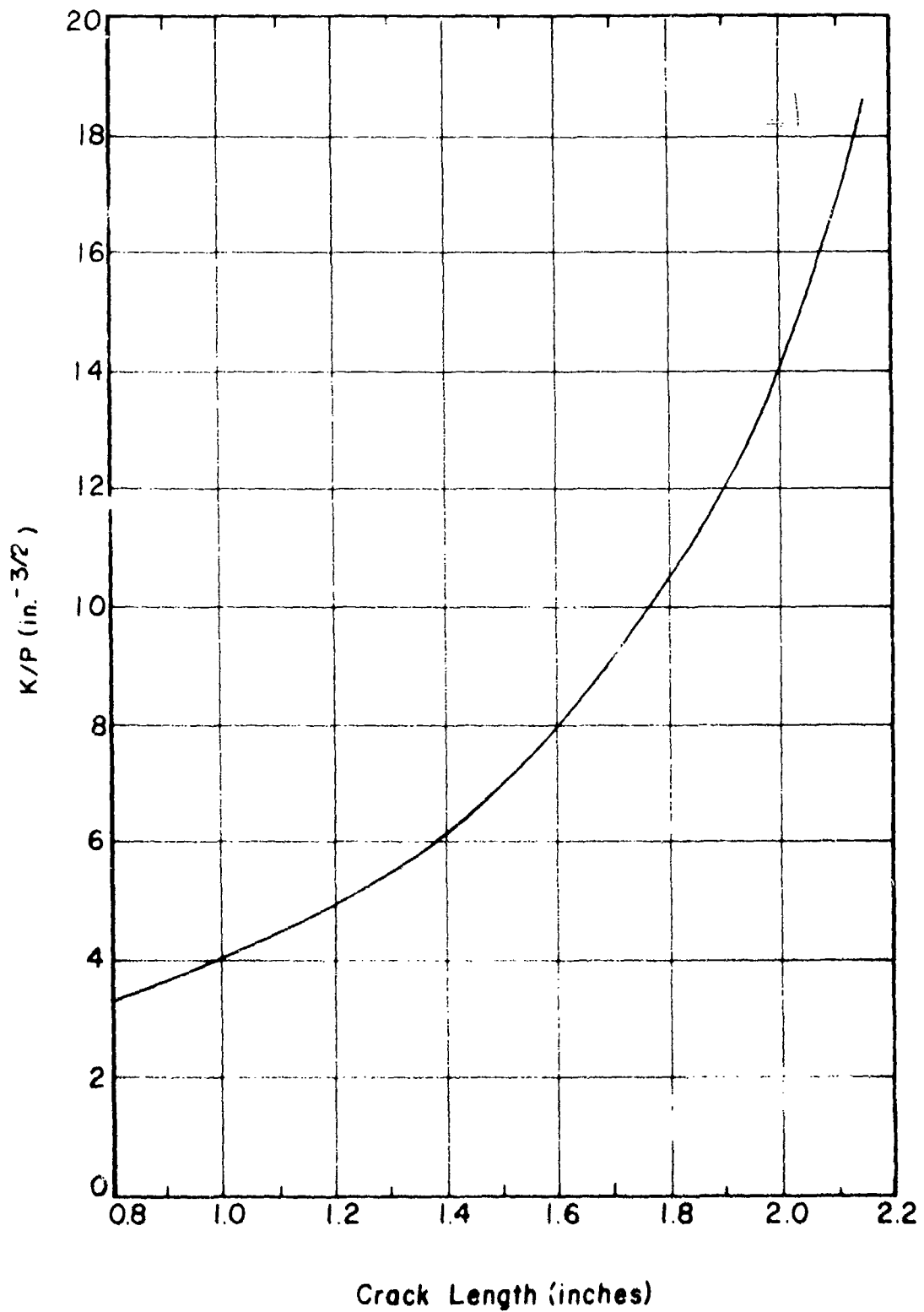
Figure 2.   Stress Intensity Factor Calibration for SEN Geometry

Loads were applied to the specimen with a mechanical test system (hydraulically actuated, servo-controlled) which had a load cell mounted in series with the specimen. The frequency of applied loading was 10 Hz for the constant amplitude (sinusoidal wave) K_{max}^{∞} = 20 ksi $\sqrt{in}$, K_{min}^{∞} = 2 ksi $\sqrt{in}$ cyclic condition and approximately 0.05 Hz (manually applied) for the overload applications. The high frequency loading and a desiccated air environment were employed to limit the influence of any moisture induced environmental action (Reference 4).

SECTION III

RESULTS AND DISCUSSION

1. CRACK GROWTH BEHAVIOR

Detailed in Figure 3 is a schematic showing the parameters that have been utilized recently (References 5, 6, and 7) to characterize the overload affected crack propagation behavior. The nonsteady state (overload affected) region is defined in terms of cycles (N^*) and distance (a^*), termed the overload affected crack length, over which the reducing effect is observed.

The observed crack growth behavior of a crack which has been subjected to a single 100 percent overload (K_{max}^{OL} = 40 ksi $\sqrt{in}$, K_{max}^{∞} = 20 ksi $\sqrt{in}$) is presented in Figures 4 and 5 for the 120 and 220 ksi yield strength levels, respectively. The data are presented in terms of an incremental movement of the crack as measured from its position immediately prior to the overload application. The data shown in Figures 4 and 5 were utilized to find N^* and a^* for each overload application. Table III contains a listing of the observed N^* and a^* parameters and the steady state crack growth rates measured outside the delay region.

The average a^* and N^* parameters calculated using the data listed in Table III directly indicate the influence of yield strength on overload delay behavior. For the 120 ksi yield strength steel, the average overload affected crack length is 16.6 mils which is traversed in approximately 33,000 cycles; the corresponding values for the 220 ksi yield strength steel are 4.6 mils and 4100 cycles. On the basis of this information, one would have to rank the 120 ksi yield strength steel superior to the 220 ksi yield strength steel for spectrum load usage due to the significant increase in the number of reduced growth rate cycles observed in this steel. Furthermore, the average steady state crack growth rates for the 120 ksi yield strength steel are approximately a factor of 2.5 lower than those associated with the 220 ksi yield strength level.

8
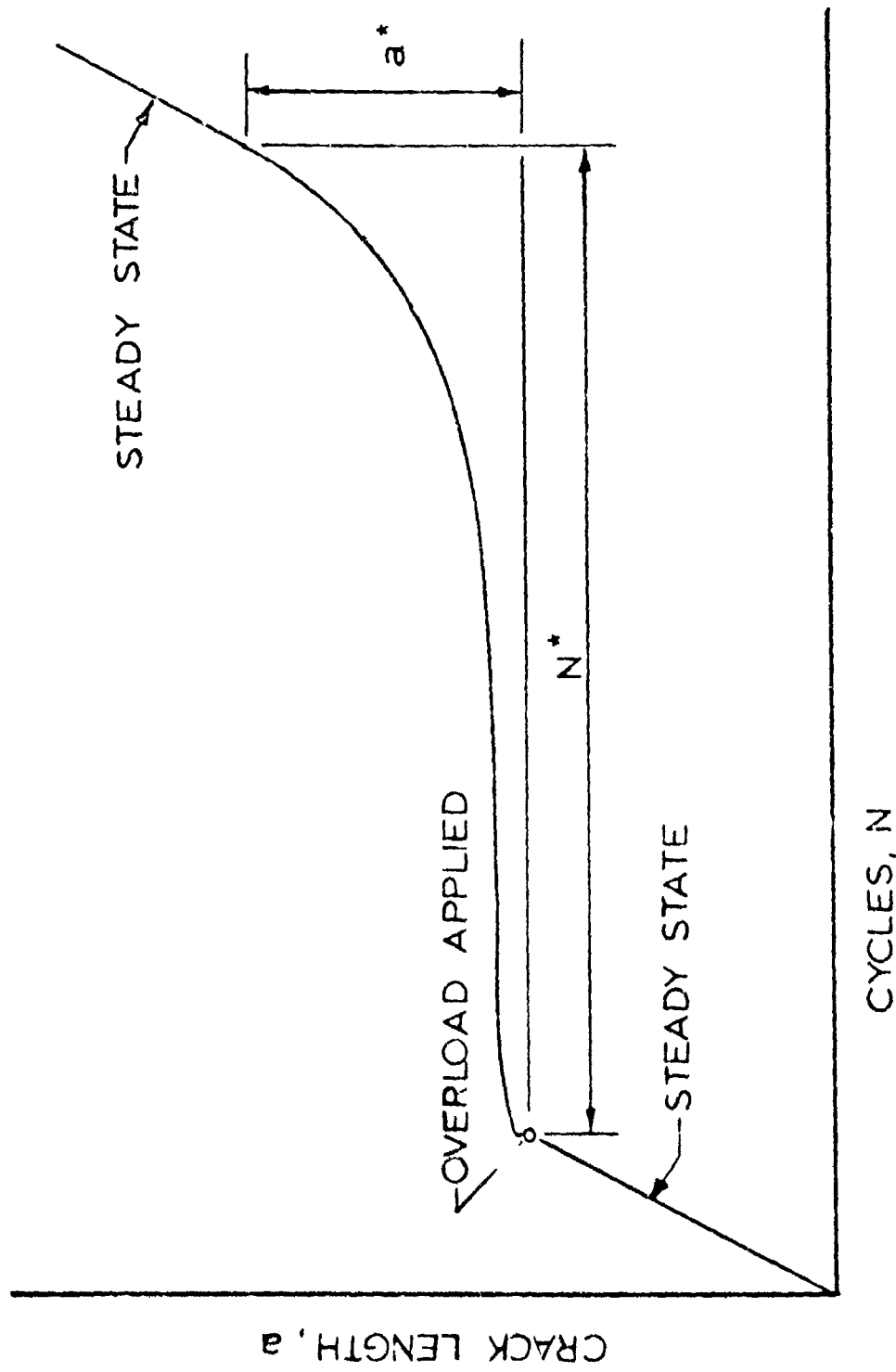
Figure 3. Schematic of Overload Affected Crack Growth Behavior

9
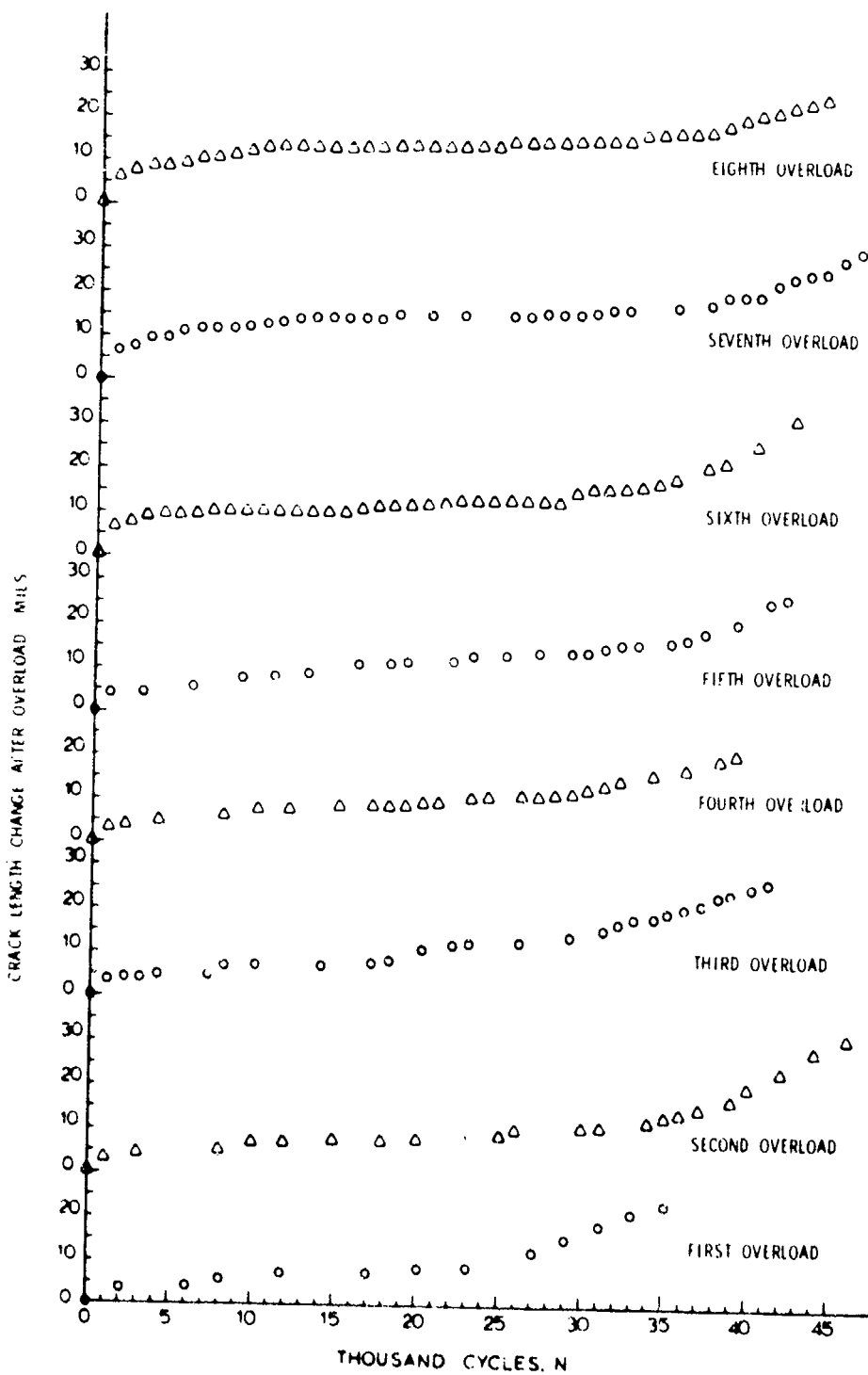
Figure 4. Overload Affected Crack Growth Behavior for 120 ksi Yield Strength 4340 Steel (Eight Overloads)
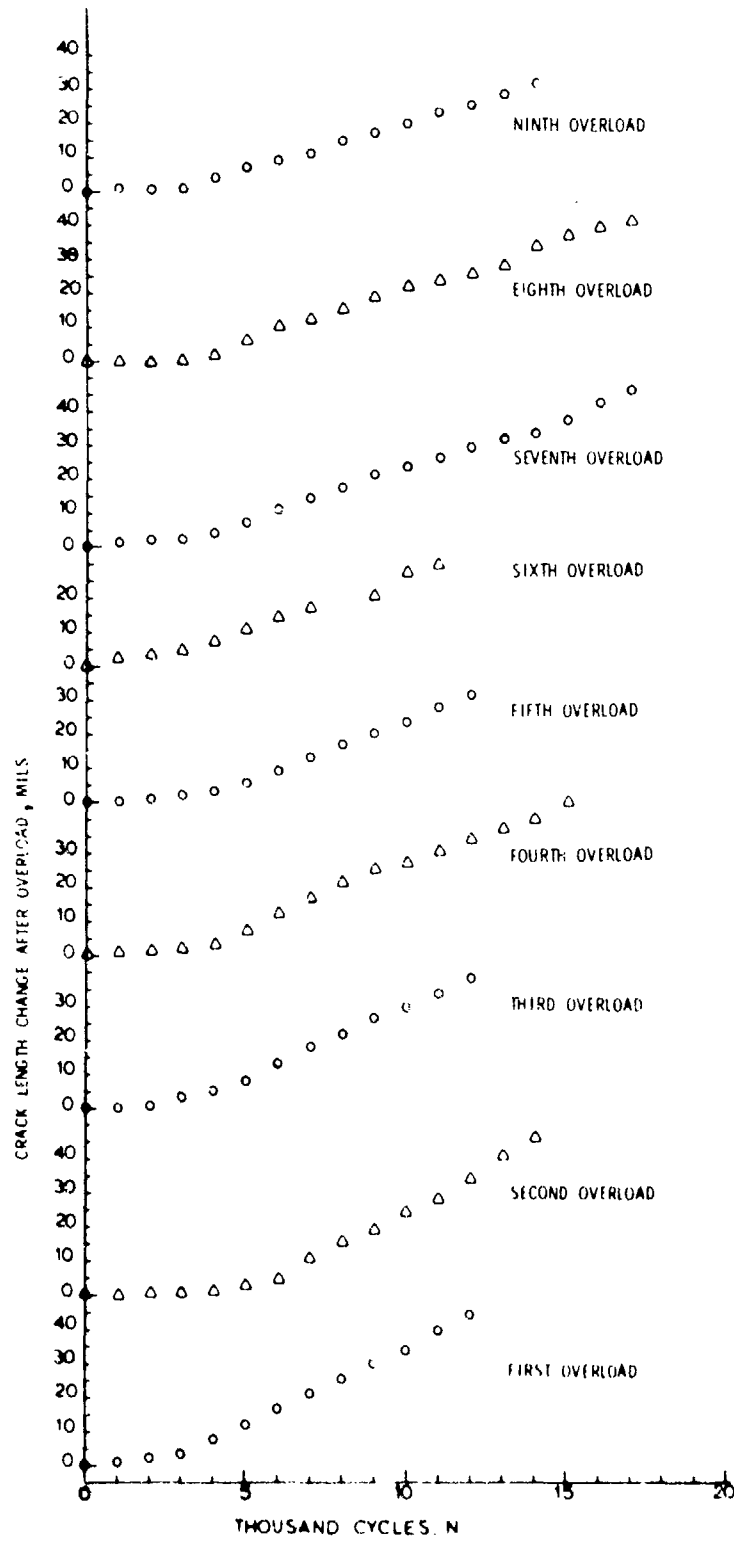
Figure 5.   Overload Affected Crack Growth Behavior for 220 ksi Yield
Strength 4340 Steel (Nine Overloads)

11

TABLE III

OVERLOAD AFFECTED ZONE PARAMETERS

$\dfrac{K_{max}^{OL}}{K_{max}^{\infty}} = 2$	120 KSI YIELD STRENGTH			220 KSI YIELD STRENGTH		
OVERLOAD	a^* mils	N^*	$\left.\dfrac{\Delta a}{\Delta N}\right|_{ss}$ 10^{-6} in/cycle	a^* mils	N^*	$\left.\dfrac{\Delta a}{\Delta N}\right|_{ss}$ 10^{-6} in/cycle
1	13	25,500	1.50	6	3800	4.71
2	16	34,500	2.06	4	5600	4.69
3	19	32,500	1.22	5	4000	4.14
4	15	30,000	0.87	4	4000	3.75
5	17	35,750	1.44	5	4900	3.70
6	17	33,500	1.83	4	2600	3.12
7	19	37,000	1.31	4	3700	3.05
8	17	36,000	1.16	5	4400	2.85
9	-	-	-	4	3900	2.66
AVERAGE	16.6	33,100	1.43	4.56	4100	3.61

$\left.\dfrac{\Delta a}{\Delta N}\right|_{ss}$ is the growth rate following overload affected growth region.

2. OVERLOAD DELAY AFFECTED CRACK LENGTH

As discussed by Gallagher (Reference 3), both Wheeler (Reference 1) and Willenborg et al (Reference 2) assumed that the overload affected crack length would be a fraction of the overload established load interaction zone (z_{OL}). Wheeler assumed that z_{OL} could be approximated by the overload created plane strain plastic zone radius while Willenborg et al utilized the overload plane stress plastic zone radius to characterize z_{OL}. The corresponding estimates of the overload affected crack length used by Wheeler and Willenborg et al are

$$a^* \leq z_{OL} \cong r^*_{y_{OL}} = \frac{1}{4\sqrt{2}\,\pi}\left(\frac{K^{OL}_{max}}{\sigma_{ys}}\right)^2 \tag{3}$$

and

$$a^* \leq z_{OL} \cong r_{y_{OL}} = \frac{1}{2\pi}\left(\frac{K^{OL}_{max}}{\sigma_{ys}}\right)^2 \tag{4}$$

respectively,

Recently, several investigators (References 5, 6, and 7) have employed variations of the following relationship (r_0 is the plastic zone diameter for the applied overload) to show good correlation with measured overload affected crack lengths

$$a^* = r_0 \cong \frac{1}{2X+6(1-X)}\left(\frac{2}{\pi}\right)\left(\frac{K^+}{\sigma_{ys}}\right)^2 \tag{5}$$

where Probst and Hillberry (Reference 7) assumed $K^+ = K^{OL}_{MAX}$ and both Von Euw et al (Reference 5) and Trebules e⁺ al (Reference 6) assumed $K^+ = K^{OL}_{max} - K^{OL}_{min}$, and X represents the fraction of the cross section exhibiting shear lips. From the fracture surfaces, X was determined to be near zero for both yield strength levels for this investigation: Equation 5 reduces to

$$a^* \cong r_0 = \frac{1}{3\pi}\left(\frac{K^+}{\sigma_{ys}}\right)^2 \tag{6}$$

for the case when X is zero

13

Table IV provides a direct comparison between the average overload affected crack lengths (a*) determined from the data given in Table III and the parameters calculated by Equation 3, 4, and 6 with $K^+ = K_{max}^{OL}$. It appears on the basis of this comparison that the Willenborg et al plane stress assumption provides the more viable approximation to the affected crack length.

TABLE IV

COMPARISON OF MEASURED AND CALCULATED AFFECTED ZONES

σ_{ys} (KSI)	a^*_{avg} (in.)	r_o (in.)	$r^*_{y_{OL}}$ (in.)	$r_{y_{OL}}$ (in.)
120	0.0166	0.0118	.00625	0.0177
220	0.00456	0.00350	.00186	0.00525

Note that the inverse ratio of the two corresponding yield strength levels squared $(220/120)^2$ closely predicts the ratio of the average measured affected crack lengths (16.6/4.6). It is expected that future observations will further substantiate this influence of yield strength (in a given material) on the size of the affected crack length.

3. WILLENBORG ET AL MODEL PREDICTED CYCLES

One test for any crack growth predictive model is its ability to predict the number of cycles of applied load to achieve a given crack length change. The Willenborg et al model as detailed by Gallagher (Reference 3) takes a form identical to that given by Equation 1 where the residual stress intensity factor K_R is defined by

$$K_R^W = K_{max}^{OL} \left(1 - \frac{\Delta a}{Z_{OL}}\right)^{1/2} - K_{max}^\infty \tag{7}$$

14

where Δa is the crack growth into the overload load interaction zone (z_{OL}). Following an overload, Δa is approximately zero and the reducing stress intensity factor is maximum. For the test conditions considered in this investigation, Equation 7 gives an initial K_R^W of 20 ksi $\sqrt{in}$. Equation 1 therefore predicts that the maximum effective stress intensity factor is zero at the crack tip.

The maximum effective stress intensity factor must be greater than the threshold (maximum) stress intensity factor (approximately 6 ksi $\sqrt{in}$ for steels when R = 0) in order that fatigue crack growth occurs. The assumption expressed by Equation 7 must be in error since Table III shows that a finite number of cycles was required to propagate the crack through the overload affected crack length. Others (References 5 through 11) have also observed that cracks grow after single overload applications where $K_{max}^{OL}/K_{max}^{\infty} \geq 2.0$, the condition for which the Willenborg et al model predicts zero crack tip (effective) stress intensity factors.

4. ALTERNATE CRACK GROWTH DELAY MODEL

A more general approach to developing the residual stress intensity factor would suggest that K_R may be proportional to the Willenborg et al residual stress intensity factor expressed by Equation 7.

$$K_R = \phi \; K_R^W \tag{8}$$

Consider the appropriate test conditions required to evaluate the proportionality factor ϕ. One boundary condition might be the "shut-off" overload to maximum load ratio $(K_{max}^{OL}/K_{max}^{\infty})$ that produces no crack growth. This would be established using techniques similar to those employed by Probst and Hillberry (Reference 7). Assume that the shut-off overload level develops a local stress intensity factor condition such that no growth is induced. Since the fatigue threshold stress intensity factor maximum $(K_{max_{TH}})$ is approximately constant for negative stress ratios (Reference 12), set the maximum local stress intensity factor (K_{max}^{eff})

15

equal to $K_{max_{TH}}$ for zero tension loading ($R = 0$). Using Equations 7 and 8, K_{max}^{eff} can be expressed as

$$K_{max}^{eff} = K_{max}^{\infty} - \phi \left(K_{max}^{OL} (1 - \frac{\Delta a}{z_{OL}})^{1/2} - K_{max}^{\infty} \right) \tag{9}$$

Immediately following the shut-off overload K_{max}^{OL} which produces no growth, $\Delta a = 0$ and $K_{max}^{eff} = K_{max_{TH}}$ and Equation 9 can be solved for ϕ subjected to these assumptions:

$$\phi = \frac{K_{max}^{\infty} - K_{max_{TH}}}{K_{max}^{OL} - K_{max}^{\infty}} \tag{10}$$

Probst and Hillberry (Reference 7) presented results in which increasing higher overloads eventually produced a condition of no crack growth for five different K_{max}^{∞} levels in 2024-T3 Aluminum. They found that the shut-off overload ratio was given by

$$K_{max}^{OL}/K_{max}^{\infty} = 2.3 \tag{11}$$

for each K_{max}^{∞} level studied.

16

5. CRACK GROWTH PREDICTIONS WITH NEW MODEL

In order to develop a estimate of the number of nonsteady state cycles (N*) associated with the overload affected zone the crack growth rates that result from each application of loading must be integrated over the overload affected zone. A Paris power law equation (Reference 13)

$$\frac{\Delta a}{\Delta N} = C\Delta K^p \tag{12}$$

was chosen as an adequate representation of the crack growth rate data for stress ratios less than 0.1 (assuming that tension only stress intensity factors establish ΔK).

The steady state crack growth equations used for predicting N* were

$$\frac{\Delta a}{\Delta N} = 1.376 \times 10^{-10} \; \Delta K_{eff}^{3.2} \tag{13}$$

for the 120 ksi yield strength steel and

$$\frac{\Delta a}{\Delta N} = 3.46 \times 10^{-10} \; \Delta K_{eff}^{3.2} \tag{14}$$

for the 220 ksi yield strength steel. The exponent 3.2 was determined from independent tests on these two steels by others (References 4 and 14) and the pre-exponential constant was selected so that Equations 13 and 14 would intersect the average steady state crack growth rates at $K = 18 \; ksi \; \sqrt{in}$ given in Table III.

The effective stress intensity ranges used in Equations 13 and 14 were obtained either by subtracting K_{min}^{eff} from K_{max}^{eff} when K_{min}^{eff} was greater than zero or by the value of K_{max}^{eff} when K_{min}^{eff} calculated using Equations 1 and 9 was less than zero.

The parameter : defined by Equation 10 was estimated on the basis of two assumptions: (1) the shut-off overload ratio for the steels investigated is close to that defined by Equation 11 and (2) $K_{max_{TH}}$ for steels is approximately 6 ksi $\sqrt{in}$ for a stress ratio of zero. Equation 10 subjected to these two assumptions becomes

$$: = \frac{1 - 6/K_{max}^{'}}{1.3} \tag{15}$$

A numerical integration approach was employed to estimate the number of applied cycles required to propagate the crack from its preoverload position to a position one plane stress (overload) yield zone radius (Equation 4) ahead of the preoverload position. One-tenth of the plane stress yield zone radius was thought to be an adequate increment in the integration scheme. Table V lists the calculations corresponding to the development of the predictions based on the new model defined by Equations 1, 7, 8, 15, and 13 or 14. Table VI summarizes the results of a *, N*, $r_{y_{OL}}$, N** (average number of N measured to achieve $r_{y_{OL}}$) and the corresponding predictions associated with both the Willenborg et al and new models. As can be discerned from Table VI, the new model predicts (to within 10 percent) the number of cycles observed to achieve $r_{y_{OL}}$. The new model is also noted to be conservative since steady state rates are predicted in a shorter number of cycles than was observed.

6. PREDICTION OF CRACK GROWTH RATES USING NEW MODEL

The crack growth data presented in Figure 4 were used to obtain the cyclic crack growth rates for the 120 ksi yield strength 4340 steel listed in Table VII. The fatigue crack growth rate data for the first five singularly applied overloads are presented graphically in Figure 6. While the magnitudes of the crack growth rates associated with each curve plotted are noted to be similar, there appears a tendency for the shape of the trough in the curve to become flatter and longer with each succeeding overload. This observation is reinforced when Table VII is used to compare the growth data for the first and second overload to that for the seventh and eighth overload. The reason for this change in crack

18

TABLE V

LIST OF CALCULATIONS FOR SURFACE OBSERVATIONS

X	ΔX	ΔK_{AVG} KSI $\sqrt{in}$	σ_{ys} = 120 KSI			σ_{ys} = 220 KSI		
			$\frac{da}{dN}$ AVG 10^{-6}in/cycle	Δa mils	ΔN	$\frac{da}{dN}$ AVG 10^{-6}in/cycle	Δa mils	ΔN
0								
	0.1	9.7	0.169	1.77	8950	0.427	0.53	1065
0.1								
	0.1	10.9	0.240	1.77	6162	0.603	0.53	733
0.2								
	0.1	12.1	0.341	1.77	4410	0.858	0.53	525
0.3								
	0.1	13.4	0.480	1.77	3182	1.208	0.53	379
0.4								
	0.1	14.8	0.655	1.77	2315	1.646	0.53	275
0.5								
	0.1	16.3	0.905	1.77	1700	2.275	0.53	202
0.6								
	0.1	17.6	1.214	1.77	1330	3.05	.53	158
0.7								
	0.05	18	1.430	0.89	620	3.60	0.26	74
0.75								
	0.25	18	1.430	4.42	3080	3.60	1.32	379
1.00								
			$\Sigma\Delta N$ = 31750			$\Sigma\Delta N$ = 3780		

TABLE VI

COMPARISON OF PREDICTED AND MEASURED DELAY PARAMETERS

Yield Strength Level $\sim$ KSI	Overload Affected Crack Length (a^*) mils	Measured Cycles to Achieve a^* (N^*)	Overload Yield Zone Radius $(r_{y_{OL}})$ mils	Measured Cycles to Achieve $r_{y_{OL}}$ (N^{**})	Predicted Cycles to Achieve $r_{y_{OL}}$	
					Willenborg et al (N_W)	New Model (N_M)
120	16.6	33,100	17.7	35,500	8	31,750
220	4.6	4,100	5.3	4,180	8	3,780

$$z_{OL} = r_{y_{OL}} = \frac{1}{2\pi}\left[\frac{K^{OL}_{max}}{\sigma_{ys}}\right]^2$$

TABLE VII

CYCLIC CRACK GROWTH RATES FOR THE 120 KSI YIELD STRENGTH LEVEL

a_Q mils	a_f mils	Δa mils	CYCLES	$\dfrac{\Delta a}{\Delta N}$ 10^{-6} in/cycle	a_{AVG} mils	CONDITION
FIRST OVERLOAD						
0	2.8*	2.8*	1	2800	1.6	Overload
0	3.5	3.5	2000	1.75	1.75	$K^{\alpha}_{max} = 20$ ksi $\sqrt{in}$
3.5	5.5	2.0	6000	0.33	4.5	
6.1	7.3	1.2	9000	0.153	6.7	
7.3	8.9	1.6	6000	0.266	8.1	
8.6	12.5	3.9	7000	0.556	10.6	
8.9	12.5	3.6	4000	0.900	10.7	
12.5	21.5	9.0	6000	1.50	15.0	
SECOND OVERLOAD						
0	3.2*	3.2*	1	3200	1.6	Overload
0	3.2	3.2	10	3.2	1.6	$K^{\alpha}_{max} = 20$ ksi $\sqrt{in}$
3.2	4.3	1.1	2000	0.55	3.75	
4.3	5.3	1.0	5000	0.20	4.8	
5.3	7.6	2.3	10000	0.23	6.45	
7.6	9.0	1.4	8000	0.17	8.3	
9.0	11.1	2.1	5000	0.42	10.05	
11.1	12.5	1.4	4000	0.35	11.8	
11.3	13.8	2.5	4000	0.62	12.55	
11.5	14.3	3.0	5000	0.60	12.8	
11.3	15.5	4.2	6000	0.70	13.4	
12.5	17.6	5.1	5000	1.02	15.05	
14.3	20.4	6.1	4000	1.52	17.35	
15.5	23.6	8.2	5000	1.74	19.95	
17.6	29.0	11.4	5000	2.	23.3	
17.6	43.9	16.4	7000	2.06	25.8	

* Based on Linear Extrapolation

TABLE VII (Continued)

THIRD OVERLOAD						
a_o mils	a_f mils	Δa mils	CYCLES	$\dfrac{\Delta a}{\Delta N}$ 10^{-6} in/cycle	a AVG mils	CONDITION
0	3.0*	3.0 *	1	3000	1.5	Overload
0	3.5	3.5	1000	3.5	1.75	K^{∞}_{max} =20 ksi $\sqrt{in}$
3.5	4.2	0.7	2000	0.35	3.85	
4.2	5.4	1.2	4000	0.3	4.8	
5.4	7.7	2.3	7000	0.33	6.55	
7.7	8.9	1.2	4000	0.300	8.3	
11.2	14.5	3.2	9000	0.356	12.85	
13.0	16.2	3.2	5000	0.64	14.6	
14.1	16.2	2.1	2000	1.05	15.1	
14.1	19.0	4.9	5000	0.98	16.5	
16.2	19.0	2.8	3000	0.93	17.6	
19.0	21.2	2.1	2000	1.05	20.1	
19.0	27.5	8.5	7000	1.22	23.2	

FOURTH OVERLOAD						
0	3.0 *	3.0 *	1	3000	1.5	Overload
0	3.3	3.3	1000	3.3	1.65	K_{max} = 20 ksi $\sqrt{in}$
3.3	3.9	0.6	1000	0.6	3.6	
3.3	5.0	1.7	3000	0.56	4.15	
5.0	6.3	1.3	3000	0.43	5.65	
6.3	8.4	2.1	7000	0.3	7.35	
8.4	9.5	1.1	5000	0.22	8.95	
9.5	11.4	1.9	6000	0.3	10.45	
11.4	12.0	0.6	3000	0.2	11.7	
11.8	13	1.2	2000	0.6	12.4	
11.8	14	2.2	3000	0.73	12.9	
12	15.1	3.1	3000	1.03	13.55	
13	15.1	2.1	2000	1.05	14.05	
14	21	7.0	8000	0.87	17.5	

* Based on Linear Extrapolation

22

TABLE VII (Continued)

FIFTH OVERLOAD						
a_o mils	a_f mils	Δa mils	CYCLES	$\dfrac{\Delta a}{\Delta N}$ 10^{-6} in/cycle	a_{AV} mils	CONDITION
0	3.9*	3.9*	1	3900	1.95	Overload
0	4.0	4.0	1000	4.	2.0	$K^a_{max} = 20$ ksi $\sqrt{in}$
4.0	5.9	1.9	5000	0.38	4.95	
5.9	8.2	2.3	5000	0.46	7.05	
8.2	12.5	4.3	11000	0.39	10.35	
12.5	14.5	2.0	5000	0.4	13.5	
14.5	15.7	1.2	4000	0.3	15.1	
15.7	17.1	1.4	4000	0.35	16.4	
16.5	17.1	0.6	2000	0.3	16.8	
16.5	18.0	1.5	3000	0.5	17.25	
16.5	19.5	3.0	4000	0.75	17.5	
17.1	19.5	2.4	2000	1.20	18.3	
17.1	27.2	10.1	7000	1.44	22.15	
SIXTH OVERLOAD						
0	5*	5*	1	5000	2.5	Overload
0	6.3	6.3	1000	6.3	3.15	$K^a_{max} = 20$ ksi $\sqrt{in}$
5	6.3	1.3	1000	1.3	5.65	
6.3	8.7	2.4	2000	1.2	7.5	
8.7	9.7	1.0	1000	1.0	9.2	
8.7	10.0	1.3	3000	0.4	9.35	
10.0	10.6	0.6	5000	0.12	10.3	
10.6	13.0	2.4	10000	0.24	11.8	
13.0	15.4	2.4	8000	0.30	14.2	
15.4	17	1.6	4000	0.40	16.2	
17	17.9	0.9	1000	0.90	17.45	
17	19.1	2.1	2000	1.05	18.05	
17.9	19.1	1.2	1000	1.20	18.5	
17.9	26.9	9	6000	1.41	22.3	
19.2	32	12.8	7000	1.83	25.6	

*Based on Linear Extrapolation

TABLE VII (Continued)

| SEVENTH OVERLOAD						
a_o mils	a_f mils	Δa mils	CYCLES	$\frac{\Delta a}{\Delta N}$ 10^{-6} in/cycle	a AVG mils	CONDITION
0	4*	4*	1	4000	2	Overload
0	4	4	1000	4	2	$K^{\infty}_{max} = 20$ ksi $\sqrt{in}$
4	7.5	3.5	2000	1.75	5.75	
6.6	11.3	4.7	4000	1.2	8.95	
9.7	12	2.3	2000	1.17	10.85	
11.3	12.5	1.2	4000	0.3	11.9	
12.5	14.8	2.3	8000	0.28	13.6	
14.8	16.3	1.5	10000	0.15	15.5	
16.3	17.5	1.2	5000	0.24	16.9	
17.5	19.0	1.5	5000	0.3	18.2	
19.5	21	2.5	3000	0.83	19.75	
19	29.7	10.5	8000	1.31	24.3	↓
EIGHTH OVERLOAD						
0	4*	4*	1	4000	2	Overload
0	6	6	1000	6	3	$K^{\infty}_{max} = 20$ ksi $\sqrt{in}$
4	8.5	4.5	4000	1.12	6.25	
6	9.3	3.3	4000	0.82	7.65	
9.3	12.2	2.9	4000	0.72	10.75	
12.2	14.5	1.8	9000	0.20	13.1	
14.6	15.1	1.1	8000	0.13	14.55	
15.1	15.5	0.4	4000	0.1	15.3	
15.5	17.8	2.4	7000	0.34	16.6	
17.5	19.2	1.7	3000	0.57	18.4	
17.5	21.0	3.5	4000	0.87	19.25	
17.9	26.0	8.1	7000	1.16	21.95	↓

*Based on Linear Extrapolation
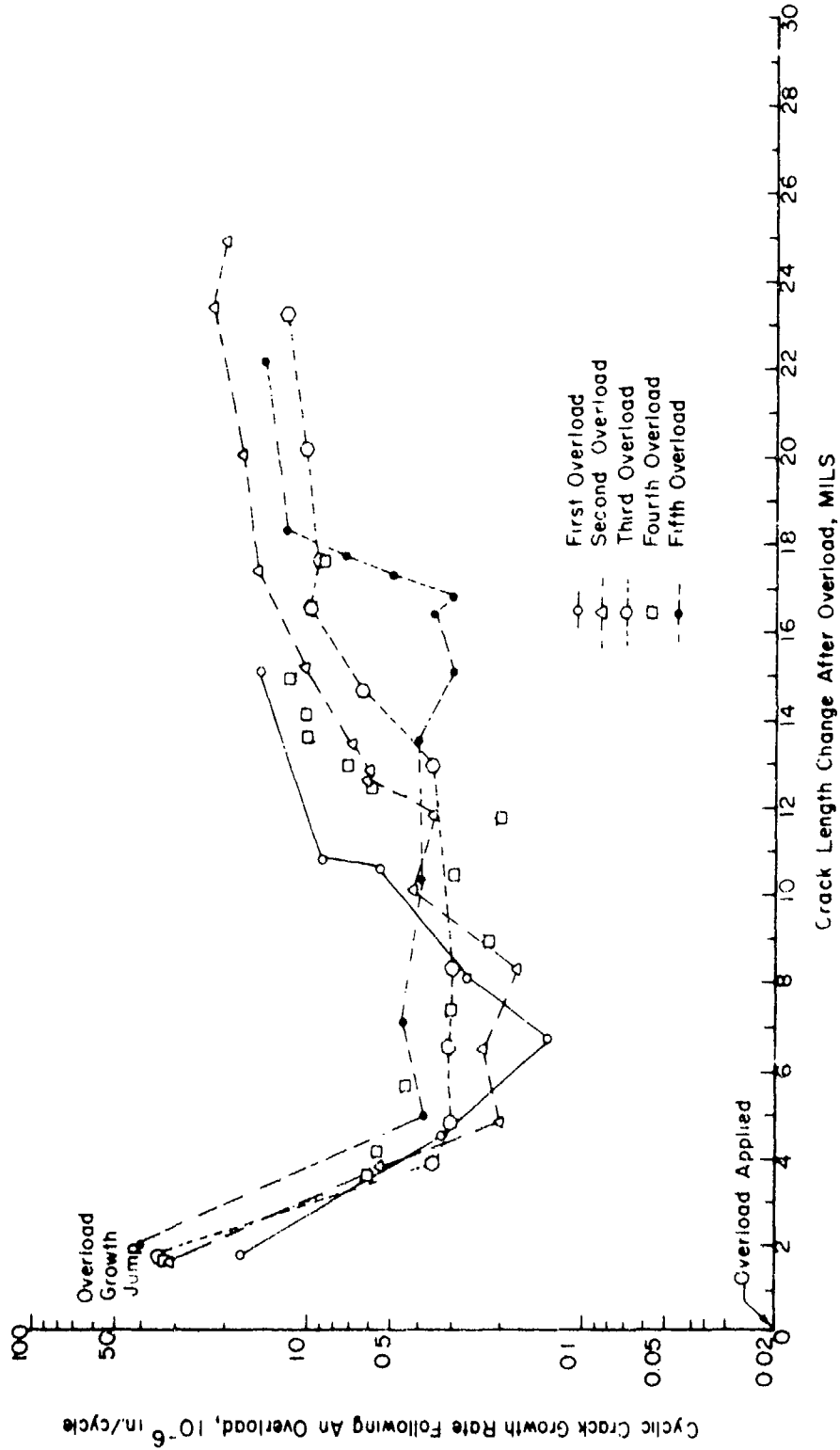
Figure 6. Crack Growth Rate Behavior Following an Overload
$[(K^{OL}_{max}/K'_{max}) = 2.]$ (First five Overloads) for 120 % Yield
Strength 4340 Steel

growth behavior with each successive overload is due to the thru-the-thickness crack front curvature changes which will be discussed below.

Table VIII provides a summary of the crack growth rate behavior for the first five singularly applied overloads as a function of the crack movement subsequent to the applied overload. These data were then used to obtain the average growth rates as a function of position for the first four and first five overloads. Table V lists the crack growth rates computed using the model as a function of incremental position in the overload affected zone. Figure 7 presents the average growth rate for the first four and first five overloads (see Table VIII) and the calculated crack growth rates for the new model.

Figure 7 shows that the observed behavior is substantially different from the model prediction in that the observed growth rates reduce gradually to their lowest level while the model predicts an abrupt change in growth behavior followed by a monotonically increasing growth rate. It can be noted that the model's monotonically increasing crack growth rate parallels the observed average growth rate behavior as it again increases to its steady state level. If the steady-state crack growth region at the end of the $r_{y_{OL}}$ (i.e. 4.7 mils) is shifted to a position prior to the beginning of the growth delay region, the model behavior closely describes the average growth rate curves (see Figure 8).

7. BELOW THE SURFACE

It was assumed that the crack growth behavior observed on the surface was identical to that which was occurring within the specimen. Failure of the specimen revealed that following the initial overload, the surface crack movement in the 120 ksi yield strength steel specimen lagged the crack movement in the center of specimen by an increasing amount with each additional overload application. Detailed in Table IX is a listing of the surface and internal crack movements as related to applied overload and constant amplitude cycles between overloads. The prior to overload application crack position on the surface and at the center of the specimen is tabulated in Table X.

26

TABLE VIII

GROWTH RATES FOR OVERLOADS I THROUGH V WITH AVERAGES *

Δa** mils	$\frac{da}{dN}\big|_{I}$	$\frac{da}{dN}\big|_{II}$	$\frac{da}{dN}\big|_{III}$	$\frac{da}{dN}\big|_{IV}$	$\frac{da}{dN}\big|_{V}$	$\frac{da}{dN}\big|_{AVG(1-4)}$	$\frac{da}{dN}\big|_{AVG\ (1-5)}$
2⁺	1.50⁺	2.28⁺	2.63⁺	2.48⁺	4.0⁺	1.60⁺	2.08⁺
3	0.80	1.01	0.89	1.01	1.8	0.93	1.10
4	0.42	0.42	0.34	0.57	0.80	0.44	0.51
5	0.27	0.205	0.30	0.49	0.38	0.32	0.33
6	0.18	0.22	0.30	0.41	0.41	0.28	0.30
7	0.17	0.21	0.30	0.33	0.45	0.25	0.29
8	0.25	0.18	0.30	0.26	0.44	0.25	0.28
10	0.47	0.40	0.32	0.27	0.39	0.36	0.37
12	1.05	0.41	0.34	0.30	0.39	0.52	0.50
14	1.32	0.81	0.52	1.02	0.37	0.92	0.80
16	1.32	1.21	0.88	0.98	0.33	1.09	0.94
18	1.32	1.59	0.94	0.98	0.96	1.21	1.15
20	1.32	1.72	1.04	0.86	1.30	1.24	1.25

* All rates are in units of 10^{-6} in/cycle

** Crack movement subsequent to overload application
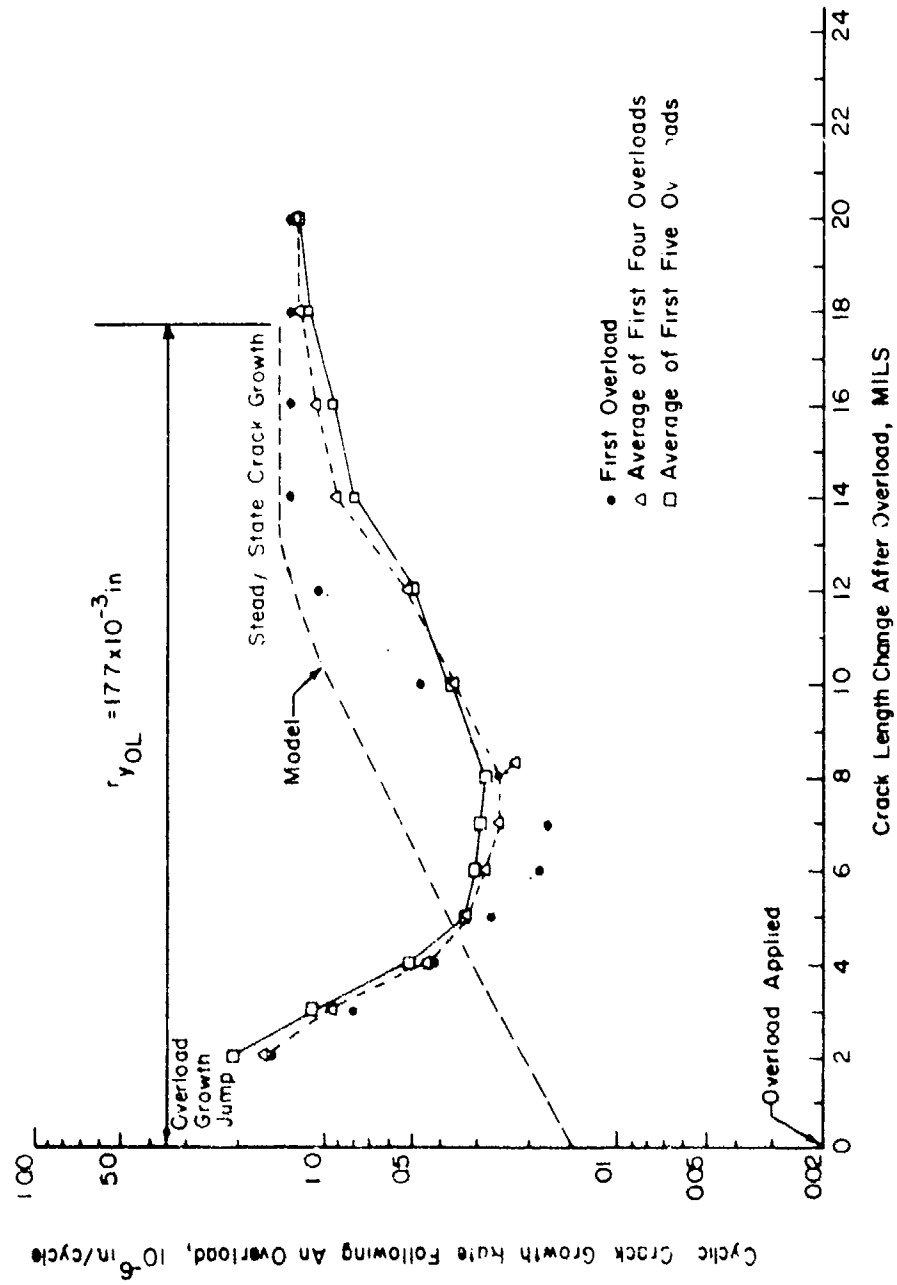
⁺ Assuming no incremental movement due to overload

Figure 7. Average Crack Growth Rate Behavior Following an Overload
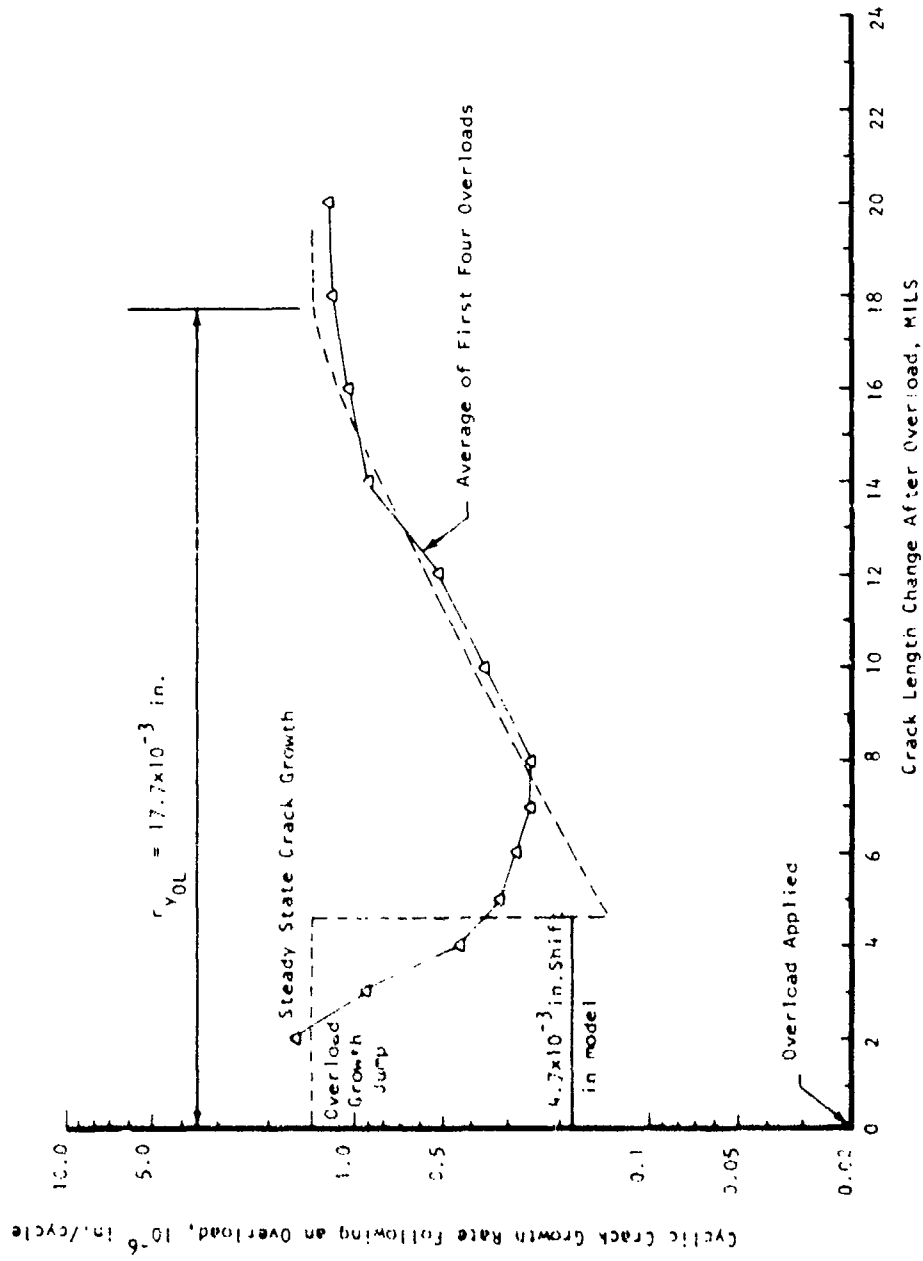$[(K_{max}^{OL}/K_{max}^{\infty} = 2.]$ Compared to Model Prediction

Figure 8. Model Prediction Applied in Reverse Order (Steady State then Nonsteady state rates) Compared to Average Behavior

TABLE IX

SURFACE AND INTERNAL CRACK MOVEMENTS BETWEEN SINGLE OVERLOADS

CRACK MOVEMENTS OBSERVED				
Overload	Δa_s** Mils	Δa_{int}** Mils	J_{int}** Mils	Cycles Between Overloads
1A*	35	47	2	30,000
1	25	39	4	35,000
2	29.5	40	3	52,000
3	27.5	38	3	42,000
4	23.5	34	2	40,000
5	27	34	2	42,000
6	40.5	38	2	41,000
7	32	38	2	46,000
8	26	38	3	43,000
AVG (1 - 8)	28.9	37.4	2.5	42,600

* Overload 1A had a reduced $K_{max}^{OL}/K_{max}^{\infty}$ of 1.8

** Δa_s, Δa_{int}, and J_{int} were the observed total surface movements, observed total internal movements, and jumps associated with the overloads.
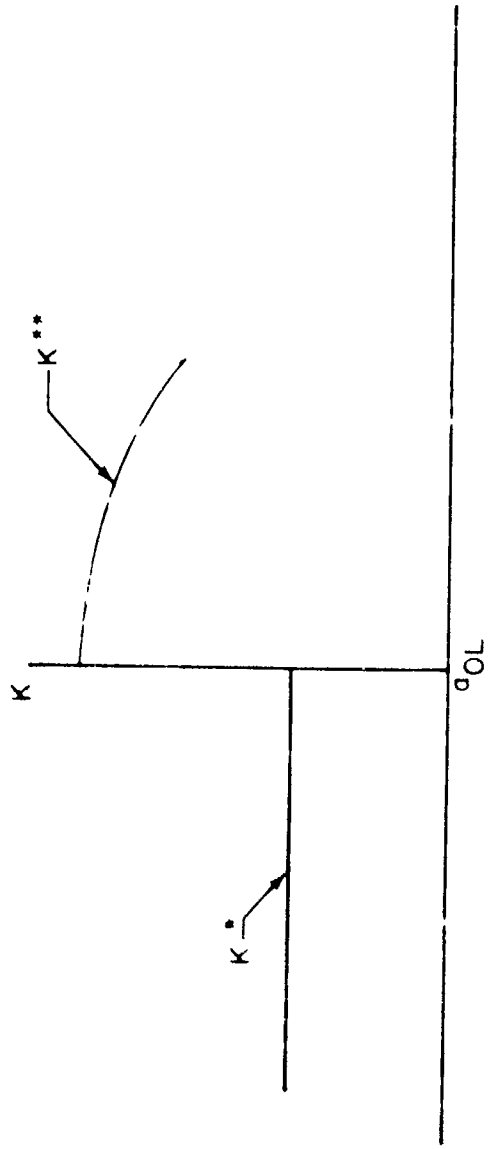
Figure 9. Schematic of No Retardation Boundary Concept to Account for Growth Jumps

TABLE X

SURFACE AND INTERNAL CRACK POSITION PRIOR TO EACH OVERLOAD APPLICATION

OVERLOAD	CRACK POSITION	
	SURFACE In.	INTERNAL In.
1A*	0.958	0.958
1	0.993	1.005
2	1.018	1.044
3	1.047	1.084
4	1.075	1.122
5	1.099	1.156
6	1.126	1.190
7	1.166	1.228
8	1.198	1.266
O.L. No. 8 PLUS 43000 CYCLES	1.224	1.304

* OVERLOAD 1A HAD A REDUCED $K_{max}^{OL}/K_{max}^{cr}$ of 1.8

Note is made in Table IX of the incremental jump in the center of specimen crack position that occurs during the overload cycle. This jump phenomenon has also been observed by Von Euw et al (Reference 4) and by Hall (Reference 15). The average crack jump during the overload was approximately 2.5 mils, approximately two orders of magnitude higher than what would have been calculated using a steady state growth rate at a $\Delta K = 40$ ksi $\sqrt{in.}$ The present model does not account for accelerated growth.

It is suspected that a generalization of the use of the load interaction zone concept (Reference 3) could be employed as a first step in modeling the jump phenomenon. For example, consider Figure 9 where the base line no retardation curve (K*) has been established for a low level loading which produces steady state growth. A high level load is applied at crack length a_{OL}, establishing a subsequent no retardation curve (K**). Assume that the incremental movement (accelerated growth) accompanying the application of the high load is related to the difference between the two no retardation curves (i.e., K* and K**). Taking the same approach that was employed in the development of the retardation model presented above, one could set the residual stress intensity factor equal to a proportionality factor multiplied by the difference in the no retardation stress intensity factors, i.e.

$$K_R = -A \ (K** - K*) \tag{16}$$

which would then be used in conjunction with Equation 1 to calculate the rate of crack advance. Insufficient evidence precludes any further discussion of the applicability of the load interaction concept as applied to overload induced crack growth acceleration.

Since the crack growth behavior obtained through surface observations is significantly different from that noted along the center of the failed specimen, it is difficult to place full confidence in the crack growth rate behavior generated using surface growth data. Possibly, there is a rather abrupt deceleration in crack advancement following an overload but this question will have to be addressed by future investigations of the delay phenomenon.

Using the internal crack tip position (see Table X) and the known applied loads employed to control stress intensity factor variables on the basis of surface measurements, it was possible to determine the change in the stress intensity factor variables associated with the mid-specimen position. The average constant amplitude stress intensity range was 19 ksi $\sqrt{in}$. It changed from 18 to 20 ksi $\sqrt{in}$ between the first overload and the last constant amplitude cycle. The average K_{max}^{∞} was 21 ksi $\sqrt{in}$, while the average K_{max}^{OL} was 42 ksi $\sqrt{in}$. Table XI provides the calculations for the retardation model behavior with the mid-stress intensity factor specimen conditions. Following the numerical integration through the overload affected zone ($a^* = 14.6$ mils) the crack was allowed to move to the average Δa_{int} position (see Table IX). The calculated number of cycles is approximately 94 percent of the average number of constant amplitude cycles applied between overloads.

TABLE XI

RETARDATION MODEL CYCLE CALCULATIONS ASSUMING
MID-SPECIMEN STRESS INTENSITY FACTOR

a' mils	Δa mils	ΔK_{AVG} ksi$\sqrt{in}$	ΔN
0	1.95	10.2	8392
1.95			
	1.95	11.5	5717
3.90			
	1.95	12.8	4058
5.85			
	1.95	14.1	2978
7.80			
	1.95	15.6	2154
9.75			
	1.95	17.2	1577
11.70			
	1.95	18.5	1249
13.65			
	0.975	19	573
14.62			
	22.8	19	13406
37.40*			
			$\Sigma\Delta N = 40104 = N_M$

* 37.40 was taken as average movement between overloads (see Table IX)
which could be associated with an average number of cycles (N_{avg}) of
42,600 to produce this growth: $N_M/N_{AVG} = .941$

SECTION IV

SUMMARY

Significant differences in delay cycles were observed when the yield strength of a 4340 steel was varied from 120 to 220 ksi. Subjecting specimens to controlled stress intensity factor conditions: single peak overloads with K_{max}^{OL} = 40 ksi $\sqrt{in}$ followed by constant amplitude cycling with K_{max}^{∞} = 20 ksi $\sqrt{in}$ (R^{∞} = 0.1), indicated that for the same external loading (e.g., spectrum loading) more retardation can be expected from a steel with lower yield strength.

Following the development of a retardation model based on overload shut-off and threshold stress intensity factor conditions, it was possible to show that a lower strength steel gives more retardation for a given loading condition primarily because its overload created load interaction zone is significantly larger.

The retardation model developed herein was found to predict to within 10 percent the cycles required to propagate a crack from its position immediately prior to overload application to a subsequent position a distance one plane stress plastic zone radius ahead of its pre-overload position. Crack growth rates obtained from surface measurements were not adequately predicted by the retardation model but note was made of similarities in predicted growth rates and observed behavior.

LIST OF REFERENCES

1. Wheeler, O. E., "Spectrum Loading and Crack Growth," Trans. ASME, Journal of Basic Engineering, Vol. 94, Series D, No.1, March 1972, p. 181.

2. Willenborg, J. D., Jr., Engle, R. M., and Wood, H. A., A Crack Growth Retardation Model Using an Effective Stress Concept, AFFDL-TM-71-1-FBR, Air Force Flight Dynamics Laboratory, Jan. 1971.

3. Gallagher, J. P., A Generalized Development of Yield Zone Models, AFFDL-TM-74-28-FBR, Air Force Flight Dynamics Laboratory, Jan. 1974.

4. Gallagher, J. P., "Corrosion Fatigue Crack Growth Rate Behavior Above and Below $K_{I_{SCC}}$ in Steels," ASTM, Journal of Materials, Vol. 6, No. 4, Dec. 1971, p. 941.

5. Von Euw, E. F. J., Hertzberg, R. W., and Roberts, Richard, "Delay Effects in Fatigue Crack Propagation," Stress Analysis and Growth of Cracks, ASTM STP 513, AM. Soc. for Testing and Materials, 1972, p. 230.

6. Trebules, V. W., Jr., Roberts, Richard, and Hertzberg, R. W., "Effect of Multiple Overloads on Fatigue Crack Propagation in 2024-T3 Aluminum Alloy," Progress in Flaw Growth and Fracture Toughness Testing, ASTM STP 536, Am. Soc. for Testing and Materials, 1973, p. 115.

7. Probst, E. P., and Hillberry, B. M., "Fatigue Crack Delay and Arrest Due to Single Peak Tensile Overloads," AIAA Paper No.73-325, presented at AIAA Dynamic Specialists Conference, March 19-20, 1973 in Williamsburg, Virginia.

8. Petrak, G. J., "Strength Level Effects on Fatigue Crack Growth and Retardation," submitted to Journal of Engineering Fracture Mechanics, 1973.

9. Jones, R. E., Fatigue Crack Growth Retardation After Single-Cycle Peak Overload in Ti-6Al-4V Titanium Alloy, AFML-TR-72-163, Air Force Materials Laboratory, April 1972.

10. Wei, R. P., Shih, T. T., and Fitzgerald, J. H., Load Interaction Effects on Fatigue Crack Growth in Ti-6Al-4V Alloy, NASA CR-2239, National Aeronautics and Space Administration, April 1973.

11. Rice, R. C., and Stephens, R. I., "Overload Effects on Subcritical Crack Growth in Austenitic Manganese Steel," Progress in Flaw Growth and Fracture Toughness Testing, ASTM STP 536, Am. Soc. for Testing and Materials, 1973, p. 95.

37

LIST OF REFERENCES (CONT)

12. Pook, L. P., "Fatigue Crack Growth Data for Various Materials Deduced from the Fatigue Lifes of Precracked Plate," Stress Analysis and Growth of Cracks, ASTM STP 513, Am. Soc. for Testing and Materials, 1972, p. 106.

13. Paris, P. C., and Erdogan, Fasil, "A Critical Analysis of Crack Propagation Laws," Journal of Basic Engineering, Trans. Am. Soc. of Mech. Engn., Series D, Vol. 85, No. 3, 1963, p. 528.

14. Gray, T. D., Unpublished Research, Air Force Flight Dynamics Laboratory (1973).

15. Hall, L. R., "Flaws at Fastener Holes" (AF Contract F33615-72-C-1740) presented at the AMS-ADP Quarterly Fracture Review, on Aug 30 and 31, 1973 at Wright-Patterson Air Force Base.